Dynamic kinesin-1 clustering on microtubules due to mutually attractive interactions

2008 Phys. Biol. 5 046004

(http://iopscience.iop.org/1478-3975/5/4/046004)

Phys. Biol. **5** (2008) 046004 (10pp) doi:10.1088/1478-3975/5/4/046004

Dynamic kinesin-1 clustering on microtubules due to mutually attractive interactions

Wouter H Roos[1,2,5,6], Otger Campàs[1,3,5,7], Fabien Montel[1], Günther Woehlke[4], Joachim P Spatz[2], Patricia Bassereau[1] and Giovanni Cappello[1,8]

[1] Institut Curie, Centre de Recherche, Laboratoire Physico-Chimie Curie, UMR168 Université Pierre et Marie Curie/CNRS/Institut Curie, 26 rue dUlm, 75248 Paris, Cedex 05, France
[2] Max-Planck-Institut für Metallforschung, Neue Materialien und Biosysteme, Heisenbergstrasse 3, 70569 Stuttgart and Universität Heidelberg, Biophysikalische Chemie, INF 253, 69120 Heidelberg, Germany
[3] Departament d'ECM, Universitat de Barcelona, Avinguda Diagonal 647, 08028 Barcelona, Catalonia, Spain
[4] Adolf Butenandt Institut, Zellbiologie, Universität München, Schillerstrasse 42, 80336 München, Germany

E-mail: Giovanni.Cappello@curie.fr

Received 14 July 2008
Accepted for publication 23 October 2008
Published 24 November 2008
Online at stacks.iop.org/PhysBio/5/046004

Abstract
Molecular motors often work collectively inside the cell. While the properties of individual motors have been extensively studied over the last decade, much less is known on how motors coordinate their action when working in ensembles. The motor collective behaviour in conditions where they contact each other, as in intracellular transport, may strongly depend on their mutual interactions. In particular, mutual interactions may result in motor clustering without the need of additional proteins. Here we study the interactions between kinesin-1 molecules by analysing their attachment/detachment kinetics on microtubules in the absence of motor motion. Our *in vitro* experiments show that kinesins-1 remain longer attached to the microtubule in the presence of neighbouring motors, resulting in the formation of motor clusters. Numerical simulations of the motor attachment/detachment dynamics show that the presence of attractive interactions between motors quantitatively accounts for the experimental observations. From the comparison of the numerical results and the experimental data we estimate the interaction energy between kinesin-1 molecules to be $1.6 \pm 0.5 K_B T$. The existence of attractive interactions between kinesins-1 provides a new insight into the coordination mechanism between motor proteins and may be crucial to understand the large scale traffic in cells.

M This article features online multimedia enhancements

1. Introduction

The motion of molecular motors such as kinesins and myosins has been studied from various perspectives. *In vitro* single-molecule motor experiments, employing techniques such as optical tweezers [1, 2], single fluorophore imaging/tracking [3, 4] and bead motility assays [5, 6] have provided insight into the mechano-chemical coupling that ultimately drives the individual motor stepping. On the other hand, approaches involving multi-motor systems have been performed in the so-called gliding assay geometry. Varying themes on such gliding assay experiments [5], with filaments sliding over structured

[5] Both authors contributed equally to this work.
[6] Present address: Natuur- en Sterrenkunde, Vrije Universiteit, 1081 HV, Amsterdam, The Netherlands.
[7] Present address: Harvard University, Harvard School of Engineering and Applied Sciences, 29 Oxford St, Cambridge, MA 02138,USA.
[8] Author to whom any correspondence should beaddressed.

surfaces [7, 8] or in the presence of an external electric field [9, 10], have also considerably contributed to the understanding of both the individual and collective behaviour of motors. In such experiments, the dynamics of the motors attached to a given filament are coupled. The 'gliding assay' geometry with kinesin motors attached to the surface and a microtubule (MT) as cargo is directly relevant for several *in vivo* situations, such as cell division, flagellar beating, etc. However, kinesin-1 motors are mainly involved in intracellular transport, where they either carry small vesicles or pull membrane tubes [11, 12]. Due to the membrane in-plane fluidity, motors typically pile up at the leading edge of the transported object, as observed for membrane tubes *in vitro* [13]. In these conditions, where the motors are close to each other, the mutual interactions might modify their collective behaviour [14] and may also affect their coordination mechanisms. Moreover, intracellular transport often takes place in the overcrowded environment of the cell, where the motors constantly interact with obstacles, among which are MT associated proteins (MAPs) and other motors. In extreme cases, the interactions between motors could even lead to jamming and disrupt the long-range transport in axons.

Electron microscopy studies showed that, in the presence of AMP-PNP (a non-hydrolyzable ATP analogue), kinesin motors do not uniformly distribute on MTs upon attachment, but tend to form clusters instead [15]. The authors in [15] concluded that contact attractive interactions between the motors had to be present to explain the observations. More recently, Seitz *et al* [16] used fluorescence microscopy to observe the motion of quantum dot-labelled kinesins in a classical bead assay geometry, and reported that the presence of an obstacle (e.g., a rigor kinesin head) induced a running motor to pause and stay attached longer to the MT. Finally, Muto *et al* [17] observed the motion of kinesin-coated beads in an *in vitro* bead assay with multiple beads. Surprisingly, their experiments suggested a long-range correlation between the beads, presumably due to a MT mediated interaction between the kinesins transporting the beads.

In spite of all the mentioned evidence for the kinesin–kinesin interaction, there is no quantitative measurement of such interaction and/or its effect on the motor kinetics. Here we study, both experimentally and numerically, the attachment/detachment dynamics of kinesins on MTs and quantitatively characterize their mutual interactions. We use fluorescence microscopy to monitor the docking of kinesin-1 motors on MTs, in the absence of motor motion. In particular, we measure the time scale of motor detachment from the MT at both high and low motor densities, and show that motors remain bound on the MT substantially longer in the presence of neighbouring motors. The kinesin pattern on the MT resulting from the attachment/detachment events is non-homogeneous, with large clusters of kinesins coexisting with regions of nearly empty MTs. Using Monte Carlo simulations we show that the experimental observations are consistent with a modification of the motor transition rates due to motor–motor attractive interactions. From the comparison between the numerical results and the measured time scales of motor attachment/detachment on MTs, we estimate the interaction energy between two neighbouring motors.

2. Materials and methods

2.1. Proteins

MTs were assembled by polymerization of tubulin purified from pig brain, and they were stabilized with 20 μM taxol. The MTs were spun in a Beckmann (Fullerton, CA, USA) TLA-100 ultracentrifuge rotor at 70 000 rpm at 37 °C for 15 min. After removal of the supernatant, MTs were resuspended in buffer *I* (80 mM Pipes-KOH, pH 6.8, containing 1 mM $MgCl_2$, 1 mM EGTA and 20 μM taxol).

HKin560, human kinesin truncated at residue 560, with an additional peptide containing a highly reactive cysteine was expressed and purified as described in [18]. Kinesins were incubated for 30 min with Cy3-maleimide (4–6-fold molar excess) for fluorescent labelling, and the reaction was stopped with 10 mM DTT. Microtubule gliding assays have shown that the kinesin activity, though reduced, persists after fluorescent labelling. Next, the motors were affinity purified by adding MTs and AMP-PNP, spinning down the MTs with bound kinesin over a glycerol layer, and then washing and resuspending the pellet in a buffer containing 5 mM ATP for detaching the active kinesins. The final concentration of HKin560-Cy3 was 2.5 $\pm$ 0.3 μM. After a final MT spin the labelled, active kinesins (not dead) are found in the supernatant. The final labelling stoichiometry, measured by spectrophotometry, is 1 $\pm$ 0.2 dyes per monomer.

2.2. PDMS pillar substrates

Microscopic, poly-dimethyl siloxane (PDMS) pillar arrays with a height of 15 μm were fabricated, as described in [8]. Briefly, the process consisted of making cylindrical cavities in SU-8 photoresist (Microchem Corp, Newton, MA, USA). Subsequently PDMS (Sylgard 184, Dow Corning, Midland, MI, USA), mixed with a thermo-crosslinker, was poured into the cavities. After curing at 65 °C for at least 4 h the PDMS block with the pillars standing on top was peeled off.

2.3. Flow cell protocol

A coverslip was dehydrated for a few minutes at 110 °C, before it was sealed onto a flow chamber made out of PDMS. Then the flow cell was connected to a syringe pump, and MTs were injected at a 5 mg ml^{-1} concentration. After 5 min incubation, to let the MTs adhere to the coverslip, the flow chamber was rinsed with a large excess of buffer *I*, and the surface was coated with casein (5 mg ml^{-1} in buffer *II*: 50 mM imidazole, pH 6.7, 50 mM NaCl, 1 mM $MgCl_2$, 2 mM EGTA and 20 μM taxol—3 min). Next a washing step with buffer *I* was performed. We finally imposed a constant flow of kinesin in buffer *I* supplemented with 1 mM AMP-PNP (Fluka, Seelze, Germany), 0.5 mg ml^{-1} casein and oxygen scavenger to reduce photobleaching (OS, 0.18 mg ml^{-1} catalase, 0.36 mg ml^{-1} glucose oxidase, 50 mM glucose). For the experiments concerning the detachment of kinesins, the solution was replaced by the motor-free buffer *I*/OS/AMP-PNP/casein.

To attach the MTs to the pillar tops an alternative protocol was used. First two stripes of double sticky tape were attached onto a cover slip, and a poly-L-lysine (Sigma-Aldrich, Buchs, Switzerland) droplet, at 0.003% wt/vol concentration, was placed in between the stripes. Subsequently, the pillar substrate was put on top and the pillars were kept in contact with the poly-L-lysine for 3 min. As a result of the hydrophobicity of the pillar substrates, a predominant coating of the pillar tops (and not the side or bottom surfaces) was achieved [8]. After incubation, the cell was rinsed thoroughly with buffer *I*, and MTs were flowed in and left to incubate for 5 min. Next, depending on the experiments, the flow cell was flushed either with 5 mg ml^{-1} of casein in buffer *II* and incubated for 3 min, or directly rinsed with buffer *I*/OS. Finally the Cy3-labelled kinesins, diluted in buffer *I*/OS containing 1 mM AMP-PNP, were flowed in. The kinesin binding was observed either directly during the injection or after rinsing with buffer *I*/OS.

2.4. Multi-FIONA approach

A sub-pixel spatial resolution of the attachment of single fluorescent kinesin motors was obtained by combining total internal reflection fluorescence (TIRF) microscopy and fluorescence imaging with one nanometre accuracy technique (FIONA) [4]. However, this technique does not work when kinesins attach at a high rate, as in our experiments. In order to overcome this problem, a high laser power was applied to induce fast bleaching of the dye. This allowed us to work under the desired conditions to measure single kinesin attachment at a resolution of two tubulin dimers. Here we refer to this technique as the 'Multi-FIONA approach'.

2.5. Imaging and data analysis

The experiments were carried out at room temperature, using a Zeiss Axiovert 200 microscope equipped with a Zeiss Plan-Apochromat 100×, NA 1.40 oil iris objective. Except for the Multi-FIONA approach, in which we used TIRF techniques, all experiments were carried out using traditional epi-fluorescence. Kinesin attachment was imaged with a CCD camera and recorded on digital DVCAM media. A home-written Matlab program was developed for the analysis of the intensity distribution along the MTs. With this program we manually tracked the position of the MT and subsequently calculated the averaged fluorescence intensity, after background subtraction, from the intensity distribution over the whole MT. Here the averaged intensity is defined as the integrated intensity per unit length of the MT.

2.6. Experiments with biotinylated K401 kinesin

The microtubules were injected in a flow chamber, previously coated with poly-L-lysine and passivated with a pre-blocking agent (casein at ∼5 mg ml^{-1}). Then, the biotinylated K401 kinesin molecules were introduced into the flow chamber in the absence of ATP. After ∼5 min, the kinesin molecules were washed out with a large quantity of buffer (few times the chamber volume). In order to reveal the kinesin molecules bound to the microtubules, a solution containing Cy3-streptavidin was then injected into the flow chamber. The flow chamber was washed with a large volume of buffer, in order to remove the free fluorescent streptavidin.

3. Results

All experiments were performed in microscopic flow cells. MTs were bound to a surface which was thereafter passivated with casein to prevent non-specific kinesin attachment. Fluorescent kinesins were injected into the chamber, and the time evolution of the fluorescence intensity on MTs was monitored by video microscopy. Each kinesin dimer was labelled with 2 ± 0.4 Cy3's (see materials and methods), so that the measured fluorescence intensity was directly proportional to the number of kinesins. In order to avoid fast photobleaching of a particular region in the observation chamber, the fluorescence evolution was recorded on different areas of the sample. A continuous steady flow of buffer, supplemented with a given concentration of motors, was imposed to ensure a constant bulk motor concentration throughout the whole experiment. We used AMP-PNP, instead of ATP, to promote the stable binding of kinesins onto MTs [19] while preventing their motion. Indeed, it is more convenient to study the interactions between immobilized motors as it avoids possible complications in the interpretation of the results coming from the motor movement. Yet, AMP-PNP is slowly hydrolyzed and the AMP-PNP kinesins detach from the MT with a characteristic time scale of several minutes [20], allowing the study of the attachment/detachment motor kinetics.

Figure 1(*A*) shows a typical time sequence of a sample of initially empty MTs kept in contact with a reservoir of kinesins at a concentration of 6 nM. There was a fast initial increase in fluorescence intensity on MTs (which lasted about 15 min; figure 1(*A*), minutes: 2–15), followed by a progressive saturation to equilibrium (at ≃38 min). We checked that, after this point, the average intensity only slightly fluctuated until the end of the experiment, 2 h later. Note that in the equilibrium state the MTs were not completely covered by kinesins (figure 1(*A*), minute: 152), consistent with the existence of detachment events at a similar time scale as the attachment of kinesins onto MTs. Moreover, kinesins were not homogeneously distributed on MTs; portions of high kinesin density alternated with regions of nearly empty MTs, in agreement with the results in [15].

Our experiments were performed at kinesin bulk concentrations ranging from 1.5 nM to 100 nM. Figure 1(*B*) shows the time evolution of the average fluorescence intensity on MTs for different bulk kinesin concentrations. The average fluorescence at each time step is obtained by averaging over many MTs in the chamber. The time scale of the motor density evolution was determined by fitting a simple exponential to the experimental data. Note that in the absence of mutual interactions of motors, beyond excluded volume, the average motor density, $\bar{\rho}$, should evolve in time according to $\bar{\rho}(t) = k_a(1 - \exp(-t/\tau))/(k_a + k_d)$ (Langmuir kinetics [21]), with $\tau = 1/(k_a + k_d)$ being the

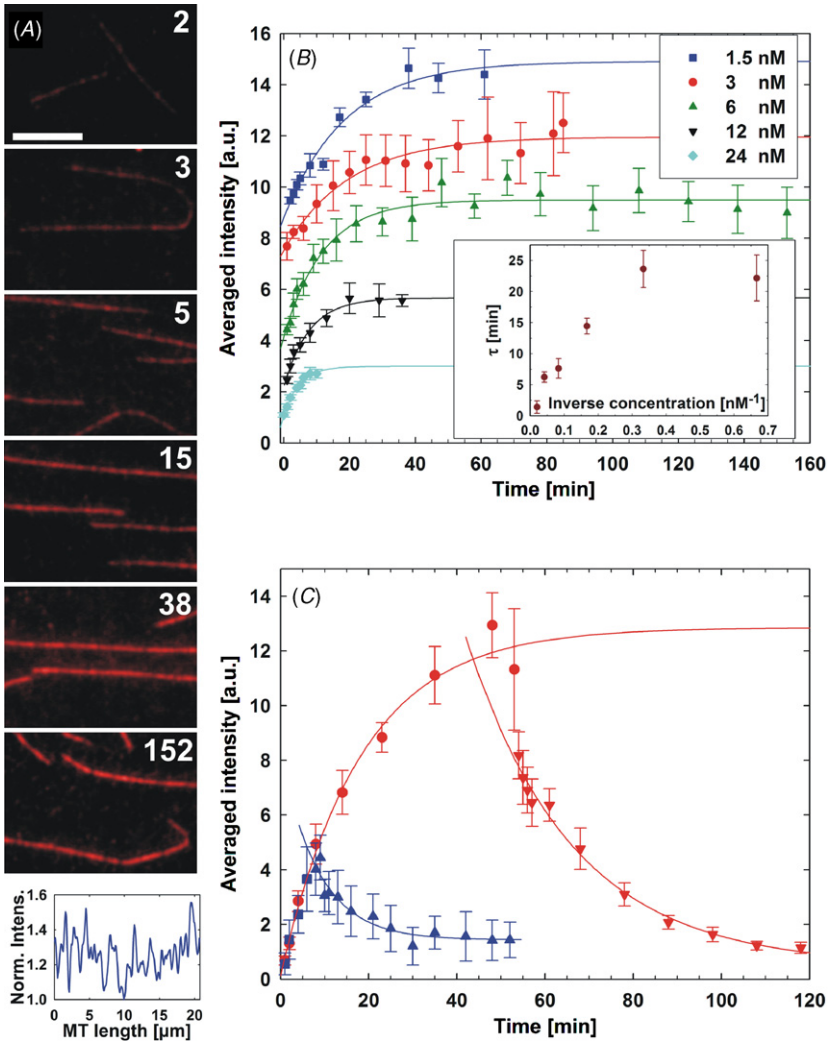

Figure 1. Kinesin attachment and detachment on MTs. (*A*) Fluorescent microscopy images showing the time evolution of the kinesin density on MTs at a bulk kinesin concentration of 6 nM. Kinesins are labelled fluorescently. Time is indicated in minutes. Bar, 5 μm. The graph below the 152 min image shows the intensity distribution (normalized by minimum intensity) along a MT of the 152 min image. (*B*) Time evolution of the average kinesin density on MTs, for different bulk kinesin concentrations, starting from empty MTs. The error bars are defined as the standard deviation in intensity at each point. Per time interval, at least an average of 9 MTs is analysed. The data for each value of bulk kinesin concentration are plotted with arbitrary y-axis units and have been shifted along this axis to include all graphs in the same figure. The continuous lines are exponential fits to the data. The inset shows the time scale of density increase, τ, as a function of the inverse of the bulk kinesin concentration, $1/\rho_{3D}$. (*C*) Decrease of the average motor density on MTs when kinesins are removed from the bulk. The initial bulk kinesin concentration before the injection of the kinesin-free buffer was 6 nM. The red plot shows the initial motor density increase (circles) followed by its decrease (triangles down) from the equilibrium motor density, when motors were removed from the bulk after approximately 50 min. The characteristic time of density decrease obtained from an exponential fit was $\tau = 24 \pm 4$ min. The blue plot corresponds to a similar experiment, but in this case kinesins were removed from the bulk when the average motor density on the MT was $\simeq$0.3 times the equilibrium value. In this case, the characteristic time of the density decrease was $\tau = 9 \pm 2$ min. Continuous lines correspond to exponential fits to the data for each situation.

characteristic time scale of the density increase, and k_a and k_d being respectively the motor attachment and detachment rates. As the attachment rate is proportional to the concentration of motors in the bulk, the time scale τ should depend on the bulk motor density ρ_{3D} as $\tau = 1/(k_d + k_0\rho_{3D})$, with k_0 being the concentration-independent attachment rate. The inset in figure 1(*B*) shows the measured values of τ as a function of $1/\rho_{3D}$. Although it qualitatively agrees with the theoretically expected form for Langmuir kinetics with only excluded volume interactions between the motors, we show below that it is not possible to account for all experimental observations (e.g., kinesin clustering) if only excluded volume interactions exist.

The images shown in figure 1(*A*) resemble images obtained by fluorescence speckle microscopy (FSM), in which the microtubules are stained with $\sim$1% of fluorescently labelled tubulin [22, 23]. With such a low concentration of fluorescent tubulin, there are on average 4 ± 2 dyes within the diffraction spot. Thus, the statistical fluctuations of the fluorescence are considerable, and the MTs appear as dotted lines. Despite some similarity, in our experiments a large amount of fluorescent kinesin is bound to the microtubules;

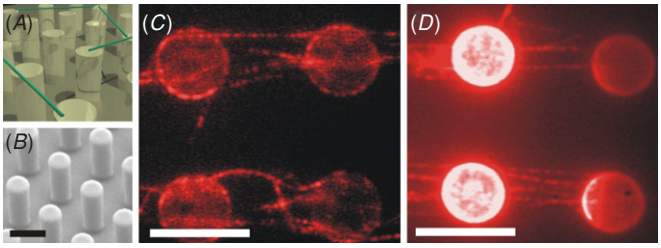

Figure 2. Kinesin patterning on freely suspended MTs. (*A*) Schematic representation of the experiment (MTs shown in green). (*B*) Scanning electron micrograph of the pillar substrate. (*C*) and (*D*) Fluorescence images of kinesin docking on MTs. Kinesin motors were labelled fluorescently and are shown in red. Kinesins were incubated for 10 min at a 30 nM bulk concentration. Images were taken after rinsing with kinesin-free buffer. The experiments were done both with (*C*) and without (*D*) casein passivation of the pillar surface and, in both cases, kinesin patterning is observed. In (*D*) the tops of the pillars appear very bright due to the non-specific binding of kinesins in the absence of casein passivation. Bar, 10 μm.

at the steady state the coverage reaches 30–40%, which corresponds to $\sim 65 \pm 8$ kinesins within the diffraction spot. Such a value has been estimated using the multi-FIONA approach, described below. At this concentration the observed clusters cannot be simply interpreted as statistical fluctuations.

Control experiments were performed to exclude possible artefacts, arising from the interaction between the MT and the surface, and/or the blocking-agent casein, that could induce kinesin clustering. For this purpose, PDMS micropillar arrays were used with a height sufficiently large to minimize the interaction between the MTs and the surface. Furthermore, the inter-pillar gap was optimized for the typical MT length, so that the MTs were free to fluctuate between the pillars and did not interact with the bottom surface (a schematic of the set-up is shown in figure 2(*A*)). The pillars used had a relatively large top surface to increase the probability of MT binding [8], as opposed to the slender type of pillars used for creating quasi-two-dimensional actin networks [24, 25], or as a scaffold for cell spreading and motility [26–29]. In addition to excluding MT–surface interactions, the pillars also allowed us to perform the experiments without supplementing the buffers with casein, which is usually needed to prevent kinesin binding on the glass coverslip. Moreover, the pillars were high enough (15 μm, figure 2(*B*)) to minimize fluorescence background signals due to kinesins unspecifically bound to the bottom surface. Figures 2(*C*) and (*D*) show that the MTs suspended between the pillars present a non-homogeneous distribution of kinesin motors. This effect was observed in both the presence (figure 2(*C*)) and absence (figure 2(*D*)) of casein. These experiments show that neither non-specific interactions of the MTs with the surface, nor the presence of casein patches absorbed onto the MTs are the cause of the observed non-homogeneous kinesin distribution on the MT. Using the biotinylated kinesin K401 from Drosophila [30], kinesin clustering was also observed under conditions where the motors were allowed to attach in the absence of a fluorescent dye. The fluorescent reporter (a Cy3-labelled streptavidin) was added at the end of the experiments to visualize the motor density along the MTs (see online supplementary material stacks.iop.org/PhysBio/5/046004). Therefore, the appearance of kinesin clusters seems to be a robust effect.

In order to exclude the possibility that the motors aggregate in the bulk and attach to the MT as a cluster we proposed a simple approach to observe the attachment process at high spatial resolution. The arrival of each single fluorescent molecule was detected using TIRF microscopy, and its position was determined by FIONA [4]. Yildiz *et al* have shown that, by collecting a sufficient number of photons, FIONA allows a single fluorophore to be localized with 1.5 nm precision. Under our experimental conditions, the dye was localized with a precision of $\sim$15 nm, which corresponds to the length of two tubulin dimers (16 nm). These experiments were performed at high laser power, which produced fast photobleaching of the dye. As a consequence, the motor fluorescence signal disappeared from the image immediately after being measured, and a second motor could be recorded in the same area. This new application of the FIONA technique, which we refer to as the 'Multi-FIONA approach', allowed for monitoring the attachment of each single motor at a high spatial resolution at near-neighbour sites, as long as there was a sufficiently long interval between the binding events. In order to discard the motors that incidentally diffused across the excitation area, without interacting with the MT, we only recorded fluorophores appearing on three or more frames. At a video rate three frames correspond to 120 ms, which is 10–100 times longer than the time required for a kinesin to diffuse across the diffraction spot. Figure 3 shows the number of attached kinesins per two tubulin dimers after 30 min measuring at a bulk kinesin concentration of 3 nM. In the online supplementary material (stacks.iop.org/PhysBio/5/046004) the movie 'Multi-FIONA-1' shows the individual spots in the field of view, together with a time-integrated movie to show where the MTs reside. Furthermore, the movie 'Multi-FIONA-2' shows the time evolution of individual kinesin attachment along one MT. The bottom image in figure 3 shows how the kinesin distribution would be imaged by traditional epi-fluorescence microscopy for a zero detachment rate of the motors. The Multi-FIONA experiments showed that only single kinesins bind to the MT. Thus they definitely exclude motor clustering in the bulk, before binding to the MT, and unexpected threshold effects in the charge coupled device (CCD sensor). In addition, the multi-FIONA approach allows us to count the total number of kinesins bound to a microtubule of a given length and, thus, to estimate the final density of motors on the MT : 65 ± 8 kinesins within the diffraction spot.

Mutually attractive interactions between kinesins provide a plausible explanation for the observations described above. The interactions between the motors can be studied by measuring differences in the motor attachment and detachment rates in the presence and absence of neighbouring motors. In order to unambiguously show the effect of mutual interactions on the motor kinetics, it is convenient to switch off attachment events.

To this end, motors were fluxed into a chamber with initially empty MTs. After a certain time, during which

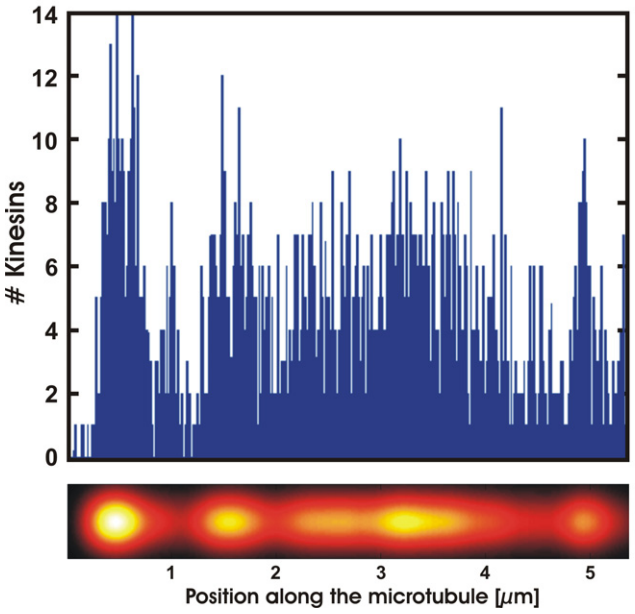

Figure 3. Kinesin binding kinetics monitored by Multi-FIONA. Number of attached motors per two tubulin dimers (16 nm) 30 min after injection as a function of the MT length (top). The bottom image shows how the MT would appear at the end of the experiment, if observed by traditional epi-fluorescence microscopy and with a zero motor off-rate. This image was obtained by convoluting the kinesin density profile measured by Multi-FIONA with the point spread function of the microscope.

the motor density increased on MTs, the motor buffer was substituted for a motor-free buffer, and the decrease in fluorescence was monitored over time by video microscopy as described previously. The removal of the motors from the bulk is done much faster (∼s) than the attachment and detachment time scales of the motors (∼min), meaning that the motors in the bulk can be removed almost instantaneously when needed. Figure 1(*C*) shows the average motor density decrease from two different initial values of the preexisting motor density on the MT. First, the system was allowed to reach equilibrium before removing the kinesins from the bulk, and the characteristic time of fluorescence decrease, τ_d, was measured to be $\tau_d = 24 \pm 2$ min (weighted average from seven experiments; mean ± sd). The experiments were then repeated, but in this case the kinesins were removed from the bulk before the system reached equilibrium, at an average density approximately 0.3 times the equilibrium value. The detachment time scale was measured to be $\tau_d = 10 \pm 2$ min (weighted average from three experiments).

If there was no effect of mutual interactions on the detachment rate of motors, the motor density would decrease exponentially in time, with a unique time scale, independent of the value of the motor density before starting the decay. However, if the time scale of motor detachment is different for motors in contact and isolated motors, one should then observe a dependence of the detachment time scale on the initial density of motors on the MT, as reported here (figure 1(*C*)).

Our experiments do not exclude the possibility that defects in the MT lattice could induce the observed motor clusters. If this was the case, however, the time scale associated with the motor–defect interaction would be hardly observable in the detachment experiments above, because the number of defects in a MT is estimated to be about 1 μm^{-1} [31]; much smaller than the number of MT lattice sites. Then, one would observe the motor density decrease to be dominated solely by the detachment time scale of motors in normal MT lattice sites. Moreover, spontaneous formation of motor clusters has been observed by electron microscopy [15] and does not appear to be caused by MT lattice defects.

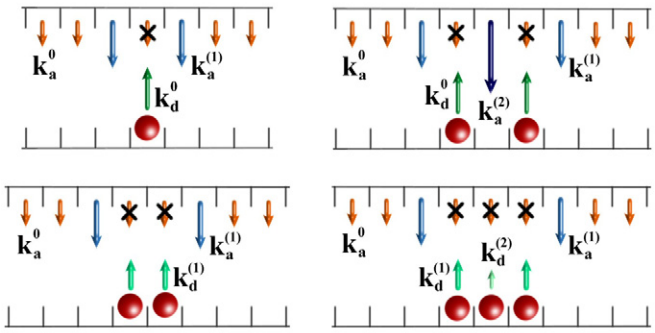

Figure 4. Motor attachment and detachment rates for different motor configurations on the MT. The mutual interactions between motors are effectively taken into account in the configuration-dependent attachment and detachment rates. The motor kinetics depends on the number of nearest neighbours as described in the main text. Rates for bound motors with empty neighbouring sites (top) and for motors in contact (bottom).

3.1. Simulations

We use here continuous time Monte Carlo simulations (see, e.g., [32]) to show that our experiments are consistent with the existence of attractive contact interactions that affect the motor attachment and detachment rates.

We consider a MT embedded in a solution of constant bulk motor density, ρ_{3D}. For simplicity, we simulate the attachment/detachment kinetics of the motors on a single protofilament, which is considered to be a one-dimensional lattice of period ℓ. Although kinesin motors are composed of two motor domains which can attach to two consecutive MT sites with different rates [15], here we consider the motor as a unit and neglect the existence of different rates for the attachment/detachment of the two distinct motor domains [33]. We show below that our experimental observations are in good agreement with this simplified description.

The motors in the bulk can attach to any site along the MT provided it is empty, and a motor bound to the MT can detach from it. The effect of mutual interactions between motors is effectively taken into account in the attachment and detachment rates (figure 4), as done previously in [15, 33]. Only contact interactions are assumed between the motors, so that a motor is only affected by the presence of motors in its neighbouring sites. A motor occupying a site with empty neighbouring sites detaches from the MT at a rate k_d^0, whereas if only one of its neighbouring sites is occupied by another motor, it detaches at a rate $k_d^{(1)} \equiv \delta k_d^0$, with δ

being a dimensionless parameter that characterizes the effect of the interaction on the detachment rate. In the case that both neighbouring sites are occupied, the detachment rate is given by $k_d^{(2)} = \delta^2 k_d^0$. A value, $\delta = 1$, characterizes a situation in which the detachment rate is not affected by the presence of neighbouring motors. The attachment rate to a site with empty neighbouring sites is k_a^0, whereas in the case only one of the neighbouring sites is occupied, the attachment rate is $k_a^{(1)} = \gamma k_a^0$. The attachment rate to a site with both neighbouring sites occupied is $k_a^{(2)} = \gamma^2 k_a^0$. The dimensionless parameter γ quantifies the effect of the motor interaction on the attachment rate.

Unlike the detachment rate, the attachment rate to a given site depends on how many motors are likely to attach to that site from the bulk. The attachment rate, k_a^0, is thus given by $k_a^0 = k_0 \rho_{3D}$; changes in the bulk motor concentration correspond to changes in the time scale for the motor attachment. The transition rates of the motors define the dynamics of the system (figure 4).

At equilibrium, detailed balance imposes [15]

$$\frac{k_a^{(1)}}{k_d^{(1)}} = \frac{k_a^0}{k_d^0} \exp\left(\frac{J_{m-m}}{K_B T}\right), \tag{1}$$

where J_{m-m} is the interaction energy between two neighbouring motors, and $K_B T$ is the thermal energy. It is then possible to estimate the interaction energy J_{m-m} if the ratio γ/δ is known as

$$\frac{\gamma}{\delta} = \exp\left(\frac{J_{m-m}}{K_B T}\right). \tag{2}$$

A ratio, $\gamma/\delta > 1$ ($\gamma/\delta < 1$), corresponds to effective attractive (repulsive) interactions, in which case $J_{m-m} > 0$ ($J_{m-m} < 0$).

The equilibrium properties of the system depend on the ratio of the rates, meaning that the relevant parameter is the ratio γ/δ and not δ and γ, separately. However, the time evolution of the system and the characteristics of the density inhomogeneities depend both on δ and γ. Specifically, in the discussion below we estimate the values of δ and γ by quantitatively comparing the time evolution observed experimentally to the results from the simulations.

4. Discussion

As described above, kinesin motors unbind from the MT with a time scale that depends on the value of the preexisting motor density on the MT. In the particular experiments performed (see results), the time scale of the fluorescence intensity decay from the equilibrium density on the MT was 24 min. When the preexisting motor density was $\simeq$0.3 times the equilibrium value, the time scale of the decay was measured to be 10 min. Assuming that the equilibrium value of the motor density on the MT, for a 6 nM kinesin bulk concentration, is large enough so that on average most bound motors have neighbours, we can identify $1/k_d^{(1)} \simeq 24 \pm 2$ min and $1/k_d^0 \simeq 10 \pm 2$ min, leading to $\delta \simeq 0.4 \pm 0.1$. Note that if in these conditions the motor density on the MT was very large, a better estimate would possibly be $1/k_d^{(2)} \simeq 24 \pm 2$, leading to $\delta \simeq 0.6 \pm 0.1$. We show below that the value $\delta \simeq 0.4 \pm 0.1$ is a reasonable estimate that allows us to quantitatively reproduce all the experimental observations.

In order to characterize the attachment events and estimate the values of k_0 and γ, we compare the simulated and experimental motor density increase from an initially empty MT, for the different motor bulk concentrations tested experimentally. In the simulations, we use the previously estimated values of $\delta = 0.4$ and $\left(k_d^0\right)^{-1} = 10$ min. The experimentally measured fluorescence intensity increase is close to an exponential relaxation to equilibrium (figure 1(*B*)). This observation sets a limitation on the possible values of γ, as for values $\gamma \gg 1$ the numerically obtained density increase deviates significantly from the exponential form. Moreover, values $\gamma < 1$ tend to smooth the density inhomogeneities (see below), which is in contrast with our experimental observations concerning cluster formation. We simulate the motor density increase on the MT and adjust the values of γ and k_0 so that the numerical results reproduce the experimental observations for all values of the motor concentration tested experimentally. In particular, in order to estimate k_0 we performed an iterative algorithm that converges and provides their values: first, we associate k_a^0 directly with the time scale of motor density increase at 50 nM (which corresponds to the attachment time scale, as at high bulk motor density the attachment rate is much larger than the detachment rate). Then, by simulating the motor density increase at different (lower) concentrations and fitting the results to the experimental data we obtain the value of γ. We then simulate the density increase at 50 nM with the previously obtained value of γ, now allowing k_0 to vary, and obtain k_0 from the fit of the density increase. The simulations are performed again for the density increase at different bulk motor concentrations with a new value of k_0 and obtain a new value for γ. By repeating this iterative scheme twice, the parameters converge respectively to $\gamma \simeq 2$ and $k_0 \simeq 8.9 \times 10^{-3}$ nM^{-1} min^{-1} (figure 5(*A*)–(*D*)). Note in particular that for $\gamma = 1$ (dashed line; figure 5(*A*)–(*D*)) it is not possible to adjust the density increase at different motor concentrations, meaning that mutual interactions not only affect the detachment rate, but also the motor attachment rate. The proposed model allows us to reproduce all the experimental data with the same, small, set of parameters (k_0, k_d^0, δ and γ), and provides a simple explanation for the observed phenomena.

With the estimated values of all the parameters, we perform the simulation of the experiments described above concerning the detachment of motors (see results and figure 1(*C*)). In figure 5(*E*), we show both the motor density increase on the MT for $\rho_{3D} \simeq 6$ nM and the density decay from the same initial densities as in the experiments shown in figure 1(*C*). The numerical results are in good quantitative agreement with the experimental observations and, in particular, they properly account for the difference in the time scale of density decrease when starting from different preexisting motor densities on the MT. Moreover, the simulations allow us to access the actual value of the motor density, ρ, expressed in units of the close-packing density $1/\ell$. For the value of the bulk motor concentration used in these particular experiments ($\rho_{3D} \simeq 6$ nM) the equilibrium average

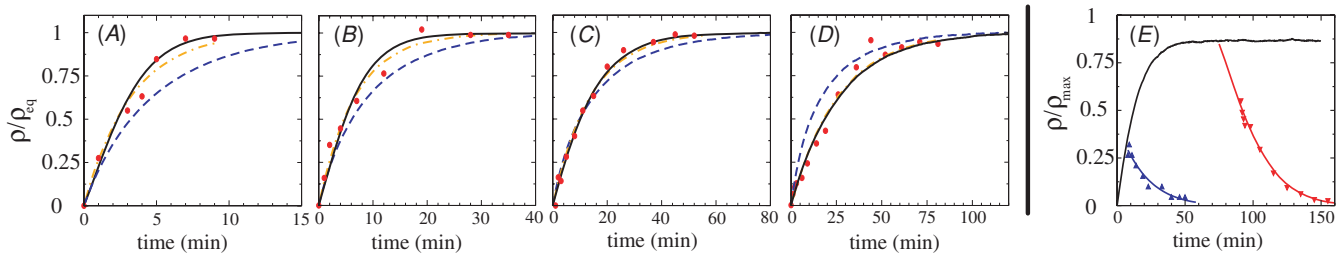

Figure 5. Comparison to the experimental data. (*A*)–(*D*) Time evolution of the average density of motors from an initially empty MT. The average density is normalized to the equilibrium value $\rho_{\rm eq}$. In all cases, $\delta = 0.4$ and $(k_d^0)^{-1} = 10$ min. The value of k_0 is obtained from the density increase at a bulk motor concentration of 50 nM and estimated to be $k_0 \simeq 8.9 \times 10^{-3}$ nM^{-1} min^{-1}. For $\gamma = 1.0$ (the blue dashed line) the numerical results do not agree with the fluorescence increase observed experimentally (red circles), whereas for $\gamma = 2$ the simulated density increase (the black continuous line) is in good agreement with the experimental data at all bulk motor concentrations tested: (*A*) 24 nM, (*B*) 12 nM, (*C*) 6 nM and (*D*) 3 nM. Note that the time evolution in the presence of interactions (the black continuous line; $\delta = 0.4$ and $\gamma = 2$) is similar to an exponential increase (the orange dashed-dotted line). (*E*) Time evolution of the average motor density field when motors are removed from the bulk at a given time. The simulations pretend to quantitatively reproduce the experiments in figure 1(*C*). The parameters used are those estimated previously, i.e. $(k_d^0)^{-1} = 10$ min, $k_0 \simeq 8.9 \times 10^{-3}$ nM^{-1} min^{-1}, $\delta = 0.4$ and $\gamma = 2$. The value of the bulk motor density (before removing the kinesins from the bulk) is $\rho_{\rm 3D} = 6$ nM, as in the experiments shown in figure 1(*C*). The experimental data for the density decrease, starting both at high (red triangles down) and low (blue triangles up) preexisting motor densities, are in good quantitative agreement with the simulated decreases (red and blue continuous lines). $\rho_{\rm max} = 1/\ell$ and corresponds to the close packing density.

density is $\rho_{\rm eq} \simeq 0.85$, meaning that most motors are in contact with other motors. Therefore, it is indeed legitimate to assume that most motors have neighbours in order to estimate the detachment rates, as we did above.

In order to further check that our parameter estimates are reasonable, we simulate the system dynamics using the estimated values and compare the properties of the density inhomogeneities to those observed experimentally. For large motor concentrations in the bulk, the MT is nearly fully covered and large density inhomogeneities are less frequent, as observed experimentally (figure 1(*A*)). We thus analyse numerically the density inhomogeneities at a fixed equilibrium average density $\rho_{\rm eq} \simeq 0.25$. Figure 6(*A*) shows the kymograph for the time evolution of the motor density field, starting from an empty MT, for different sets of parameters of special interest. The kymograph is a two-dimensional representation of the time-dependent density field, in which the motor density is colour coded. Regions with no motors appear black, whereas high-density regions appear white. The local density is obtained by averaging the occupation number in the simulations over 15 sites. We show the case with only excluded volume interactions between the motors ($\delta = 1, \gamma = 1$; figure 6(*A*)). If only the detachment rate depends on the mutual interactions ($\delta = 0.4, \gamma = 1$; figure 6(*A*)) between motors, small clusters of motors can be observed, and their lifetime is longer than that of the small inhomogeneities observed in the presence of only excluded volume interactions. On the other hand, when only the attachment rate depends on the mutual interactions ($\delta = 1.0, \gamma = 2.0$; figure 6(*A*)), cluster formation is also enhanced, but the lifetime of the motor clusters is short and, in particular, smaller than for $\delta = 0.4$. In the general case where both the attachment and detachment rates are affected by the interactions ($\delta = 0.4, \gamma = 2.0$; figure 6(*A*)), the motor clusters are larger and persist longer on the MT than in the preceding cases. The large density inhomogeneities observed experimentally are thus consistent with the presence of attractive interactions affecting both the attachment and detachment rates, in accordance with our results above.

These qualitative observations concerning the density inhomogeneities can be made quantitative by analysing the statistical properties of the motor density inhomogeneities. The variance of the density values along the MT provides a quantitative measure of the magnitude of the inhomogeneities. In figure 6(*B*) we plot the variance of the motor density relative to the average density as a function of time, $\mathrm{var}_\rho(t)/\bar{\rho}(t)$, for a bulk motor density of 1.5 nM. The numerical results clearly distinguish the cases with only excluded volume interactions between the motors ($\gamma = 1, \delta = 1$; figure 6(*B*), the dashed black line), and that with mutually attractive interactions for the previously obtained values of γ and δ ($\gamma = 2.0, \delta = 0.4$; figure 6(*B*), the continuous red line). The experimentally observed evolution of the relative variance (figure 6(*B*), dots) quantitatively agrees with the simulated evolution with mutually attractive interactions. These results, in agreement with the findings described above, confirm the presence of contact attractive interactions between the motors as a reasonable explanation for the observed clustering phenomena.

Although the actual values of δ and γ may differ slightly from our estimates, our results suggest that both the attachment and detachment rates are affected by the presence of mutual interactions of motors. Varying the values of the parameters within a reasonable range, we find that the actual values of δ and γ for which the simulation results are in fairly good agreement with the observations are $0.3 < \delta < 0.6$ and $1.5 < \gamma < 2.5$.

Finally, knowing the estimates for both δ and γ we can evaluate the interaction energy, $J_{m-m} = K_B T \ln(\gamma/\delta)$, between the motors, as follows from equation (2). We obtain $J_{m-m} = 1.6 \pm 0.5 K_B T$. This energy, which adds to the interaction between the kinesin and the MT, leads to a significant increase of the time that a motor remains bound to the MT in the presence of neighbouring motors. In particular,

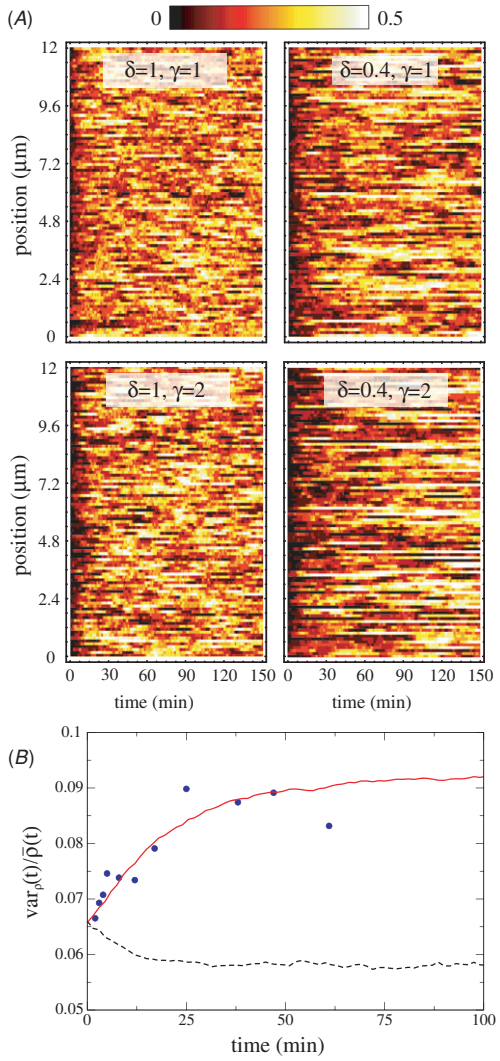

Figure 6. Characteristics of the density inhomogeneities. (*A*) Kymographs representing the time evolution of the motor density field from an initially empty MT. Kymographs correspond to the smoothing of the original data at the microscope resolution. In all cases, the saturation average density is fixed to $\rho_{\rm eq} \simeq 0.25$ and $(k_d^0)^{-1} = 10$ min. The different kymographs correspond to different values of δ and γ, and are discussed in the main text. A density scale between 0 and 0.5 is used to increase the contrast between regions with no motors and high-density regions. The density inhomogeneities are more important for larger values of γ and smaller values of δ, corresponding to mutually attractive interactions between the motors. (*B*) Time evolution of the variance of the density along the MT relative to its average value. The values of k_d^0 and k_0 are those estimated experimentally: $(k_d^0)^{-1} = 10$ min and $k_0 \simeq 8.9 \times 10^{-3}$ nM^{-1} min^{-1}. Also the bulk motor density has been chosen as in the experiment, $\rho_{3D} = 1.5$ nM. If only excluded volume interactions exist between the motors ($\gamma = 1, \delta = 1$; the dashed black line), the relative density variance decays as a function of time until it reaches a constant value. In contrast, for the previously estimated values of δ and γ ($\gamma = 2.0, \delta = 0.4$; the continuous red line), corresponding to contact attractive interactions, the relative variance increases at short times to eventually saturate, as observed experimentally ($\rho_{3D} = 1.5$ nM; dots). The intensity scale is arbitrary, because the experiments do not supply its absolute value. The experimentally observed time evolution is quantitatively reproduced by the simulations (for $\gamma = 2.0$ and $\delta = 0.4$) and cannot be explained, even qualitatively, by only excluded volume interactions.

this time is increased by a factor of about 6 if a motor is in between two neighbouring motors.

5. Conclusion and outlook

The present work studies the mutual interactions between kinesin-1 motors through the dynamics of kinesin docking onto MTs. We report the formation of dynamic kinesin clusters on MTs and show that the kinesin detachment rate from the MT depends on the presence of neighbouring motors. The simulations of the motor kinetics, in the presence of mutual interactions, show that our experimental observations are compatible with attractive interactions between the motors. According to our framework, the kinesin clustering is due to a simultaneous enhancement of the motor attachment rate and reduction of their detachment rate in the presence of neighbouring motors. The quantitative comparison of the experimental data and the numerical results allows us to estimate the interaction energy between motors to be $1.6 \pm 0.5 K_B T$.

Although out of the scope of the present work, the origin of this interaction and the mechanism by which it affects the motor kinetics are interesting questions. The increase of the attachment rate in sites neighbouring already bound motors is particularly puzzling. The presence of a bound motor could locally change the MT lattice, thereby favouring the attachment via a MT-mediated interaction [34]. It is also possible that upon attachment the motors diffuse over the MT lattice in a weakly bound state. The likeliness of attachment would increase in the presence of an already bound motor. This one-dimensional diffusion on the MT lattice has already been observed for other motors of the kinesin family such as KIF1a [35], MCAK [36] and Eg5 [37].

The importance of motor cluster formation in cellular systems is apparent in the cooperative action of motors during vesicle transport and membrane tube formation. Motors work in small groups where they frequently contact each other. The mutually attractive interactions may not only drive the formation of these motor clusters but also help coordinating the activity of the motors within the cluster. Moreover, the cluster formation reported here is likely to translate into traffic jam formation in the presence of ATP. However, further investigation is needed to elucidate the role of the ATP hydrolysis on the dynamics of these inhomogeneities.

Acknowledgments

We thank Chantal Tassius, Cécile Leduc, Jacques Prost, Yariv Kafri, Andrea Parmeggiani, Erwin Frey and Paolo Pierobon for valuable discussions. We thank the financial support of the European Network PHYNECS (HPRN-CT-2006-00312) (O C), the Spanish M E C (O C), the European BIOMACH Program (G C) and the EU-STREP BIOMICS (J P S and G C).

Glossary

Multi-FIONA: fluorescence imaging with one nanometre accuracy used to detect the position of multiple spots simultaneously.

References

[1] Schnitzer M J, Visscher K and Block S M 2000 Force production by single kinesin motors *Nat. Cell Biol.* **2** 718–23

[2] Mehta A D, Rief M, Spudich J A, Smith D A and Simmons R M 1999 Single-molecule biomechanics with optical methods *Science* **283** 1689–95

[3] Vale R D, Funatsu T, Pierce D W, Romberg L, Harada Y and Yanagida T 1996 Direct observation of single kinesin molecules moving along microtubules *Nature* **380** 451–3

[4] Yildiz A, Forkey J N, McKinney S A, Ha T, Goldman Y E and Selvin P R 2003 Myosin V walks hand-over-hand: Single fluorophore imaging with 1.5-nm localization *Science* **300** 2061–5

[5] Vale R D, Schnapp B J, Reese T S and Sheetz M P 1985 Organelle, bead, and microtubule translocations promoted by soluble factors from the squid giant-axon *Cell* **40** 559–69

[6] Cappello G, Badoual M, Ott A, Prost J and Busoni L 2003 Kinesin motion in the absence of external forces characterized by interference total internal reflection microscopy *Phys. Rev.* E **68** 021907

[7] Romet-Lemonne G, VanDuijn M and Dogterom M 2005 Three-dimensional control of protein patterning in microfabricated devices *Nano Lett.* **5** 2350–4

[8] Roos W, Ulmer J, Grater S, Surrey T and Spatz J P 2005 Microtubule gliding and cross-linked microtubule networks on micropillar interfaces *Nano Lett.* **5** 2630–4

[9] Riveline D, Ott A, Julicher F, Winkelmann D A, Cardoso O, Lacapere J J, Magnusdottir S, Viovy J L, Gorre-Talini L and Prost J 1998 Acting on actin: the electric motility assay *Eur. Biophys. J.* **27** 403–8

[10] van den Heuvel M G L, Butcher C T, Smeets R M M, Diez S and Dekker C 2005 High rectifying efficiencies of microtubule motility on kinesin-coated gold nanostructures *Nano Lett.* **5** 1117–22

[11] Hirokawa N 1998 Kinesin and dynein superfamily proteins and the mechanism of organelle transport *Science* **279** 519–26

[12] Vedrenne C and Hauri H P 2006 Morphogenesis of the endoplasmic reticulum: beyond active membrane expansion *Traffic* **7** 639–46

[13] Leduc C, Campas O, Zeldovich K B, Roux A, Jolimaitre P, Bourel-Bonnet L, Goud B, Joanny J F, Bassereau P and Prost J 2004 Cooperative extraction of membrane nanotubes by molecular motors *Proc. Natl. Acad. Sci. USA* **101** 17096–101

[14] Campas O, Kafri Y, Zeldovich K B, Casademunt J and Joanny J F 2006 Collective dynamics of interacting molecular motors *Phys. Rev. Lett.* **97** 038101

[15] Vilfan A, Frey E, Schwabl F, Thormahlen M, Song Y H and Mandelkow E 2001 Dynamics and cooperativity of microtubule decoration by the motor protein kinesin *J. Mol. Biol.* **312** 1011–26

[16] Seitz A and Surrey T 2006 Processive movement of single kinesins on crowded microtubules visualized using quantum dots *EMBO J.* **25** 267–77

[17] Muto E, Sakai H and Kaseda K 2005 Long-range cooperative binding of kinesin to a microtubule in the presence of ATP *J. Cell Biol.* **168** 691–6

[18] Lakamper S, Kallipolitou A, Woehlke G, Schliwa M and Meyhofer E 2003 Single fungal kinesin motor molecules move processively along Microtubules *Biophys. J.* **84** 1833–43

[19] Bloom G S, Wagner M C, Pfister K K and Brady S T 1988 Native structure and physical-properties of bovine brain kinesin and identification of the ATP-binding subunit polypeptide *Biochemistry* **27** 3409–16

[20] Hancock W O and Howard J 1999 Kinesin's processivity results from mechanical and chemical coordination between the ATP hydrolysis cycles of the two motor domains *Proc. Natl. Acad. Sci. USA* **96** 13147–52

[21] Fowler R H 1936 *Statistical Mechanics* 2nd edn (Cambridge: Cambridge University Press)

[22] Waterman-Storer C M and Salmon E D 1998 How microtubules get fluorescent speckles *Biophys. J.* **75** 2059–69

[23] Danuser G and Waterman-Storer C M 2006 Quantitative fluorescent speckle microscopy of cytoskeleton dynamics *Ann. Rev. Biophys. Biomol. Struct.* **35** 361–87

[24] Roos W H, Roth A, Konle J, Presting H, Sackmann E and Spatz J P 2003 Freely suspended actin cortex models on arrays of microfabricated pillars *Chemphyschem* **4** 872–7

[25] Mohrdieck C, Wanner A, Roos W, Roth A, Sackmann E, Spatz J P and Arzt E 2005 A theoretical description of elastic pillar substrates in biophysical experiments *Chemphyschem* **6** 1492–8

[26] Rovensky Y A, Bershadsky A D, Givargizov E I, Obolenskaya L N and Vasiliev J M 1991 Spreading of mouse fibroblasts on the substrate with multiple spikes *Exp. Cell Res.* **197** 107–12

[27] Tan J L, Tien J, Pirone D M, Gray D S, Bhadriraju K and Chen C S 2003 Cells lying on a bed of microneedles: an approach to isolate mechanical force *Proc. Natl. Acad. Sci. USA* **100** 1484–9

[28] du Roure O, Saez A, Buguin A, Austin R H, Chavrier P, Siberzan P and Ladoux B 2005 Force mapping in epithelial cell migration *Proc. Natl. Acad. Sci. USA* **102** 2390–5

[29] Steinberg T, Schulz S, Spatz J P, Grabe N, Mussig E, Kohl A, Komposch G and Tomakidi P 2007 Early keratinocyte differentiation on micropillar interfaces *Nano Lett.* **7** 287–94

[30] Surrey T, Elowitz M B, Wolf P E, Yang F, Nedelec F, Shokat K and Leibler S 1998 Chromophore-assisted light inactivation and self-organization of microtubules and motors *Proc. Natl. Acad. Sci. USA* **95** 4293–8

[31] Davis L J, Odde D J, Block S M and Gross S P 2002 The importance of lattice defects in katanin-mediated microtubule severing in vitro *Biophys. J.* **82** 2916–27

[32] Newman M E J and Barkema G T 1999 *Monte Carlo Methods in Statistical Physics* 1st edn (Oxford: Clarendon)

[33] Frey E and Vilfan A 2002 Anomalous relaxation kinetics of biological lattice-ligand binding models *Chem. Phys.* **284** 287–310

[34] Krebs A, Goldie K N and Hoenger A 2004 Complex formation with kinesin motor domains affects the structure of microtubules *J. Mol. Biol.* **335** 139–53

[35] Okada Y and Hirokawa N 2000 Mechanism of the single-headed processivity: diffusional anchoring between the K-loop of kinesin and the C terminus of tubulin *Proc. Natl. Acad. Sci. USA* **97** 640–5

[36] Helenius J, Brouhard G, Kalaidzidis Y, Diez S and Howard J 2006 The depolymerizing kinesin MCAK uses lattice diffusion to rapidly target microtubule ends *Nature* **441** 115–9

[37] Kwok B H, Kapitein L C, Kim J H, Peterman E J G, Schmidt C F and Kapoor T M 2006 Allosteric inhibition of kinesin-5 modulates its processive directional motility *Nat. Chem. Biol.* **2** 480–5